Universidad de Valladolid
Faculty of Science
Cellular Materials Laboratory
Condensed Matter Physics Department

Master Thesis:

Master in Molecular Nanoscience and Nanotechnology

Study of the process-density-structure relationship in low density nanocellular materials based on PMMA.

Presented by:

Judith Martín de León

Supervisor:

Prof. Miguel Ángel Rodríguez Pérez

Valladolid, Julio 2016

Financial Support

Financial assistance from, (MAT 2012 – 34901) MINECO, FEDER and UE (MAT2015-69234-R) and the Junta de Castile and Leon (VA035U13) are gratefully acknowledged. Financial support from Junta of Castile and Leon grant Q4718001C (J. Martín-de León) is gratefully acknowledged.

Agradecimientos

Con estas líneas me gustaría agradecer a todas aquellas personas que han puesto su granito de arena para que este trabajo sea posible, en especial;

Por dar forma al castillo de arena, gracias a mi director Miguel Ángel Rodríguez Pérez.

Por todas las ayudas prestadas, gracias a todos y cada uno de los miembros de CellMat.

Por no cejar en su empeño de construir a mi lado no un castillo cualquiera, sino el más alto y más bonito que pueda existir, gracias a mi compañera y amiga Victoria Bernardo.

0 Resumen en Español

0.1 Introducción

La sociedad actual demanda materiales ligeros así como de materiales cuyas propiedades estén diseñadas específicamente para cada aplicación. Los materiales celulares, gracias a las propiedades que presentan, son unos excelentes candidatos que cumplen con ambas exigencias.

Los materiales celulares son materiales bifásicos, formados por una matriz sólida, y una fase gaseosa. Este estudio se centra en materiales celulares basados en una matriz sólida polimérica. Estos presentan bajas densidades, lo cual permite reducir la cantidad de materia prima utilizada así como reducir el peso. Por otra parte son materiales de bajo coste, y sus propiedades pueden ser diseñadas a la carta para cada aplicación. Por todas estas razones estos materiales están presentes en industrias como la automoción, la aeronáutica, energías renovables, etc., y el interés que existe por ellos es creciente.

En los años 80 se dio el gran salto en esta área con el paso desde los materiales celulares convencionales a los materiales microcelulares (pasando de las 300 µm de tamaño de celda a las 50µm), lo cual supuso una gran mejora de las propiedades mecánicas. El siguiente paso es la reducción del tamaño de celda por debajo de la micra, para dar lugar a lo que se conoce como materiales nanocelulares.

Los materiales nanocelulares se conocen por presentar tamaños de celda del orden de unos cientos de nanómetros, y lo que se espera de ellos es realmente prometedor. Estos materiales presentan una muy buena respuesta mecánica, además su reducido tamaño de celda les convierte en unos fantásticos aislantes térmicos gracias a lo que se conoce como efecto Knudsen. También se espera que la fabricación de materiales nanocelulares a partir de polímeros amorfos con tamaños de celda por debajo de los 50nm pueda dar lugar a materiales celulares transparentes. Todo ello les convierte en excelentes candidatos para la fabricación de aislantes para construcción, materiales con elevada rigidez y resistencia específica, materiales para filtros, elementos para catálisis y un sinfín de otras aplicaciones.

Por todo ello la producción de estos materiales, así como el control de su densidad y estructura celular con el objetivo final del control de sus propiedades, es uno de los temas de estudio hoy en día en la ciencia de los materiales.

El proceso que ha resultado más satisfactorio para la fabricación de estos materiales es lo que se conoce como “Proceso de disolución de gas”. Este proceso consiste en tres pasos, saturación, desorción y espumado. Durante la saturación el polímero es sometido a ciertas condiciones de presión de CO_2 y temperatura. En este periodo el gas difunde dentro del polímero hasta alcanzar la saturación. Una vez que el material ha saturado, se procede a una rápida liberación de la presión. Esto provoca que el polímero pase a un estado de súper-saturación, en el cual el gas atrapado

dentro del polímero forma lo que se conoce como puntos de nucleación. Por último, en la etapa de espumado, el polímero se sumerge en unos baños térmicos a una temperatura superior a la temperatura de transición vítrea efectiva, otorgando una elevada movilidad a las cadenas poliméricas, lo cual permite que los puntos de nucleación crezcan formándose las celdas del material celular en cuestión.

Como se puede ver, el proceso de fabricación de estos materiales nanocelulares, depende de multitud de parámetros (presión y temperatura de saturación, velocidad de relajación de la presión, tiempo de desorción, temperatura y tiempo de espumación), los cuales, afectarán a la estructura final del material y por tanto a sus propiedades.

El principal objetivo de este estudio será la optimización de estos parámetros para la producción de espumas nanocelulares de baja densidad fabricadas a partir de un polímero puro como es el Polimetilmetacrilato (PMMA). Además se pretende encontrar la relación proceso-estructura-propiedades realizando un estudio detallado que no se ha llevado a cabo hasta la fecha, con el objetivo de obtener un control de la estructura final del material celular por medio de cambios en los parámetros de proceso.

0.2 Resultados

Este estudio describe cuales son las condiciones de proceso necesarias para producir materiales nanocelulares de baja densidad basados en PMMA. Tras optimizar los parámetros de proceso se han obtenido materiales nanocelulares con tamaños de celda entre 200 y 250nm y densidades de nucleación mayores de 10^{14} núcleos/cm^3. El rango de densidades relativas (densidad del material dividida por la densidad del material de partida) conseguidas es muy amplio, desde 0.45 hasta valores realmente bajos de 0.25. Normalmente, para alcanzar datos como este se han utilizado copolímeros, así como materiales con nanopartículas, o bien se han usado unas condiciones de saturación extremas, como temperaturas de saturación por debajo de los 0ºC, pero nunca antes se habían alcanzado valores en los rangos encontrados en este trabajo con un homopolímero sin aditivar como es el PMMA.

De acuerdo con previos resultados[1,2], se han fijado unas condiciones de saturación y despresurización que aseguran la absorción de una cantidad suficiente de gas por parte del material. Esto dará lugar a la producción de suficientes puntos de nucleación. Para la optimización final de los materiales se ha llevado a cabo un estudio los parámetros de espumado. Así pues las condiciones de saturación han sido de 31MPa de presión y 25ºC de temperatura, obteniendo de esta forma un 31% de CO_2 absorbido. Por su parte el ratio de despresurización ha sido de 100MPa/s. Por último los parámetros de espumado se han modificado variando la temperatura de espumado de 10ºC en 10ºC, desde los 40ºC hasta los 110ºC y se han usado tiempos de espumado de 1, 2 y 5 minutos para cada temperatura usada.

Una vez fabricados estos materiales, se ha llevado a cabo un estudio detallado, tanto de su densidad como de su estructura celular, con el objetivo de encontrar una clara relación proceso-

densidad-estructura. Para ello se han analizado todos los parámetros que definen la estructura celular, dividiendo el estudio en dos partes, parámetros que definen las características de la fase gaseosa y parámetros que definen las características de la fase sólida. En cuanto a la fase gaseosa se han analizado parámetros como el tamaño de celda, la densidad de nucleación y el porcentaje de celda abierta. Mientras que para la caracterización de la fase sólida se ha analizado el espesor de pared y la fracción de masa en las aristas.

Este análisis ha llevado a obtener información detallada de cómo afectan los parámetros de proceso a la estructura final del material celular. Así pues se ha encontrado que el incremento de temperatura y tiempo de espumado provocan una disminución de la densidad relativa del material, hasta los 110ºC, temperatura que parece ser el límite superior de fabricación de estos materiales. Por otra parte en cuanto a la estructura, un aumento de la temperatura y el tiempo de espumado no producen un efecto significativo en el tamaño de celda, no siendo así para la densidad de nucleación, la cual se ve incrementada en un factor dos cuando se pasa de bajas a altas temperaturas de espumado. Por otra parte, en cuanto a la fase sólida se refiere, se ha concluido que el espesor de pared permanece también constante, con valores muy bajos de 25nm, mientras que la fracción de masa en las aristas disminuye conforme aumenta la temperatura y el tiempo de espumado. Todos los cambios que se observan en la estructura celular, tienen una clara relación con la reducción de la densidad relativa. Es por ello que se ha concluido que un aumento de la temperatura y el tiempo de espumado dan como resultado la reducción de la densidad del material celular que se traduce en un aumento en la densidad de nucleación así como una disminución de la fracción de masa en las aristas.

Se han estudiado también parámetros adicionales como la interconexión de la fase gaseosa, viendo que ésta aumenta con la reducción de densidad. Por último el efecto de confinamiento, que se puede detectar a través de un incremento de la temperatura de transición vítrea del material nanocelular frente al sólido de partida, ha sido confirmado para estas estructuras, observándose una dependencia del mismo con la densidad de los materiales.

0.3 Conclusiones

A lo largo de esta tesis de master se han fabricado materiales nanocelulares de baja densidad basados en polimetilmetacrilato, mediante la optimización de los parámetros de espumado del proceso de disolución de gas. Se ha obtenido un amplio rango de densidades relativas, abarcando desde los 0.47 para 40ºC de temperatura de espumado hasta densidades relativas de 0.24 para 90ºC. Estas bajas densidades se han obtenido por primera vez usando como materia prima un homopolímero como es el PMMA y sin usar condiciones extremas de temperaturas de saturación. Se ha llevado a cabo un análisis completo de la estructura celular, tanto de la fase gaseosa como de la sólida, correlacionando los cambios encontrados con los cambios en densidad. Se ha realizado por primera vez para estos materiales un estudio detallado de la relación proceso-densidad-estructura. De esta forma se ha concluido que el factor clave para la reducción de la densidad de este tipo de materiales es el aumento de densidad de nucleación. También se ha demostrado que la reducción de densidad provoca un incremento del contenido de celda abierta

del material así como una reducción de la fracción de masa en las aristas. Finalmente se ha confirmado que este tipo de estructuras presentan confinamiento del material en las paredes de las celdas, hecho que provoca un aumento de la temperatura de transición vítrea del material con respecto a la del material sólido.

Los resultados de este trabajo han sido enviados para publicar a la revista Polymers, el trabajo enviado recientemente y en proceso de evaluación tiene por título. Low density nanocellular polymers based on PMMA produced by gas dissolution foaming: fabrication and cellular structure characterization.

1 Abstract

This master thesis describes the processing conditions needed to produce low density nanocellular polymers based on polymethylmethacrylate (PMMA).Materials produced present relative densities between 0.45 and 0.25, cell sizes between 200 and 250 nm and cell densities higher than 10^{14} cells/cm^3. To produce these nanocellular polymers the processing parameters of the gas dissolution foaming technique, using CO_2 as blowing agent, have been optimized. Saturation conditions have been chosen to be 31MPa for saturation pressure and 25ºC for saturation temperature. These conditions allow dissolving a 31% of gas for all the materials. On the other hand depressurization ratio was fixed as 100MPa/s. Finally foaming parameters have been modified from 40ºC to 110ºC for the foaming temperature and from 1 to 5 minutes for the foaming time. Foaming temperatures in the range of 80 to 100ºC and foaming times of 2 minutes allow producing nanocellular polymers with relative densities as low as 0.24. Moreover cellular structure has been studied in-depth to obtain the process-density-cellular structure relationships. It has been found that increasing foaming temperature and time results in a decrease in relative density. It was demonstrated that this reduction is related with some changes in the final cellular structure as an increase in the cell nucleation density or a reduction in the fraction of mass in the struts. Finally, it was proved that the glass transition temperature depends on the cellular structure, being possible to measure an increment of this temperature in the cellular materials with respect to the bulk material. This effect is associated to a confinement of the polymer into cell walls.

2 Introduction

2.1 Framework of this thesis

Today's society demands both, lightweight materials as well as materials with properties specifically designed for each application. Thanks to their properties, cellular materials are good candidates for this aim. Cellular materials can present low densities that allow a reduction of the raw material needed, as well as a reduction in weight. Also its low cost, and its excellent properties, that can be customized for each application, make these materials essential for different technological areas such as, automotive sector, aeronautics, renewable energies, building, packaging, biotechnology, etc. [3,4]

For these reasons the study and production of new cellular materials with improved properties is an interesting topic in material science. One important topic in this area is the development of new cellular materials presenting a significant reduction of cell size. In the 80s conventional cellular materials took the leap towards microcellular materials (from 300 µm of cell size to 50µm). The next step consists on reducing the cell size below the micron, producing what it is known as nanocellular materials.

Nanocellular materials are really interesting ones, they present improved mechanical properties comparing to conventional cellular materials,[5,1,6] in addition to this, they could be transparent if they are fabricated from amorphous materials and the cell size is reduced below 50nm. In addition, t they are good candidates for filters or sensor. Also the reduction in the thermal conductivity that they present, due to Knudsen effect, make them suitable for thermal insulation. [7]

The importance of these materials is reflected in the UE program "Horizon 2020". One of the topics on this program is the "Fabrication and control of nanoporous materials". According to the UE: "Thanks to the large amount of applications that can be benefited with the reduction of cell size, there exists an increasing interest in nanocellular materials".

For all these reasons this thesis is based on the optimization of the production of nanoporous materials and the control of its cellular structure.

2.2 State of the art

2.2.1 Cellular material

Cellular materials consist of two-phase structures. A continuous solid or liquid phase, called matrix, and a gaseous phase that can be continuous or discontinuous[8] (Figure 1). Cellular materials can be distinguished by the type of matrix, which can be metallic, glassy, ceramic… (Figure 1) This study is focused in cellular polymers, i.e cellular materials produced from a polymeric matrix [9,3].

Cellular polymers present interesting properties making them suitable for different application such as thermal insulation, structural applications, filtration, acoustic absorption, etc[8]. These properties largely depend on the cellular structure.

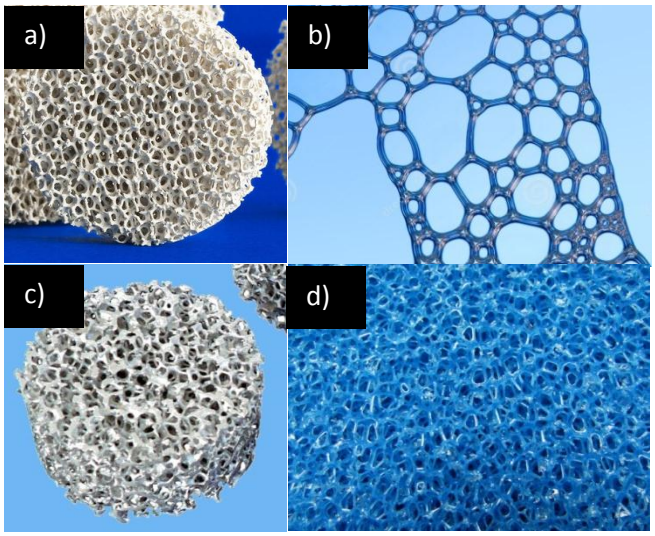

FIGURE 1. (**a**) Ceramic foam. (**b**) Aqueous foam. (**c**) Metal foam. (**d**) Polymer foam.

In order to characterize the internal structure of these materials there exist multiple descriptors of cellular materials, which are defined below.

2.2.1.1 Descriptors of cellular materials

There exist some parameters usually used to describe the structures of these materials.

Relative Density, ρ_r

Relative density (ρ_r), represents the ratio between the density of the cellular material (ρ_f) and the density of the solid precursor (ρ_s) as it is shown in Equation 1.

$$\rho_r = \frac{\rho_f}{\rho_s} \qquad [1]$$

Cell size, ϕ

This is one of the most important parameter in order to define the cellular structure. It refers to the mean diameter of the pores in the cellular material. In order to give a more complete description cell size distribution (i.e the number of cells of each size in a cellular material) as well as the standard deviation (SD) of the distribution are also used to describe more precisely the structure.

Anisotropy Ratio, AR

This value is calculated as the ratio of the cell size in a given direction (ϕ_x) and the cell size in a direction perpendicular to it (ϕ_z) as it is shown in Figure 2.

$$AR = \frac{\phi_x}{\phi_z}$$

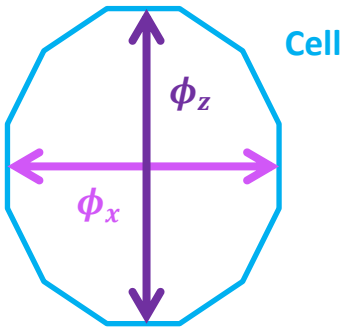

FIGURE 2. Anisotropy ratio.

Cell density, N_v

Cell density is the number of cells per unit of volume of the cellular material. It is defined in Equation 2, where n is number of cells in the analyzed image and A is the image area in cm^3. This magnitude is a three dimensional correction of a two dimensional value and it is based on the Kumar's theoretical approximation[10].

$$N_v = \left(\frac{n}{A}\right)^{\frac{3}{2}} \qquad [2]$$

Cell nucleation density, N_0

Cell nucleation density, N_0, is defined as the number of nucleation sites per unit of volume of the solid precursor. This value can be calculated from the cell density and the relative density, according to Kumar method,[10] as shows Equation 3.

$$N_0 = \frac{N_v}{\rho_r} \qquad [3]$$

Open cell content, OC

The percentage of open cells (OC %) is defined as the volume fraction of interconnected cells

Cell wall thickness, ξ

As it can be seen in Figure 3, some different parts can be distinguished in the solid part of a cellular material. Cell walls are defined as the solid part that divides two different cells. The cell wall thickness is the thickness of these elements measured in the central area of the wall.

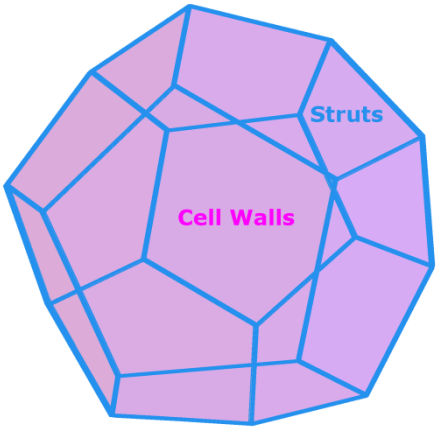

FIGURE 3. Diagram of the different elements of the solid phase in a cellular material.

Fraction of mass in the struts, f_s

Struts are defined as the sum of vertexes and edges as it is shown in Figure 3. Fraction of mass in the struts is defined as the ratio between the amount of solid material located at struts (vertexes and edges) and the total amount of solid material. It is given by Equation 4:

$$f_s = \frac{m_{struts}}{m_{struts} + m_{walls}} \qquad [4]$$

2.2.1.2 Cellular materials classification

Cellular materials can be classified attending to different parameters of those defined previously; attending to the relative density cellular materials can be classified in two types, cellular materials presenting $\rho_r > 0.6$ are considered **high density materials**, while materials presenting $\rho_r < 0.3$ are **low density ones**. This classification is really useful because, it is well known that cellular materials' properties (P_f) depend on the property of the bulk material (P_s) and also on its density as shows Equation [5]:

$$P_f = C\, P_s \left(\frac{\rho_f}{\rho_s}\right)^n \qquad [5]$$

Where C takes values near 1 and the value of n varies between 1 and 2 and depends on the cellular structure and the property under study.

On the other hand, cellular materials can be also classified according to their open cell content, i.e. their degree of interconnections between cells. Materials with completely isolated pores are known as **closed cell cellular materials**, those that present an interconnected structured are said to present **open cell structures**. Finally, one of the most used classifications is the one that refers to cell size, **macro-cellular materials** are those with cell sizes larger than 100 μm, **microcellular**

materials characterized by cell sizes below 100 μm, and **nanocellular materials**, those studding in this thesis, with cell sizes In the nanometric range (lower than 1 μm).

2.2.2 Nanocellular materials

The research on cellular polymers is a popular topic in material science. But the real evolution in this field can be found since the development of microcellular polymers in the 80s at Massachusetts Institute of Technology (MIT).[3] As it has been said microcellular polymers are characterized by cell sizes below 100 μm and also present cell densities around 10^9 cells/cm^3. These materials are well known multiphasic systems. Several studies analysing the fabrication and characterization of microcellular materials using different polymers as solid phase can be found in the bibliography. Materials such as polysulfone (PSU),[11] polystyrene (PS),[12] polyvinyl (chloride) (PVC),[13] polyurethane (PU),[14] polyethylene (PE),[15] polymethylmetacrylate (PMMA),[16] polycarbonate (PC)[17] have been used for this purpose. The reason that justifies the increasing interest for these systems relies on the improvement in the mechanical properties that they present in comparison with macro-cellular materials. For example they present better tensile and impact properties than conventional cellular materials. This improvement has been also proved in different polymeric systems such as poly (ethylene terephthalate) (PET),[18] acrylonitrile butadiene styrene (ABS),[19] Polyvinyl chloride (PVC) [20,] or Polycarbonate (PC) [21].

The next step in the direction of improving the properties of these materials is the development of nanocellular polymers. Nanocellular polymers are characterized by cell sizes in the nanometric range and cell nucleation densities higher than 10^{14} cells/cm^3. [5,22] These materials are expected to present interesting properties, they could have better mechanical properties than microcellular ones and really low thermal conductivities. In fact, the high potential of these materials has been recently proved for different systems. On the one hand, D Miller et al. have proved that the reduction of cell size to the nanoscale in PEI foams results in an increase in the strain to failure and tensile toughness.[6] In addition, it has been proved that nanocellular PMMA presents higher modulus of elasticity, higher impact strength and improved hardness than microcellular PMMA.[1] On the other hand, another interesting fact recently proved for nanocellular PMMA is that cell size reduction allows decreasing the thermal conductivity thanks to Knudsen effect [23,24].

These materials are of great interest for the industry due to the interesting properties that they present. For these reasons the optimization of the production process is a topic under study in the last few years.

2.2.2.1 Fabrication techniques of nanocellular materials

Several methods have been proposed in the last years to produce nanocellular polymers. For instance pattern-transfer techniques have been used to obtain thin film nanocellular polymers.[25] One example of these pattern-transfer techniques is the solvent based technique in which nanocellular polymers are produced from block copolymers with thermally stable blocks and thermally labile blocks. So that it is possible to selective removal of one of the blocks. The thermally labile blocks are removed by using organic solvents leaving nanopores behind.[26] Also

there exist other techniques suitable to produce nanostructured materials such as; phase separation techniques,[27,28] colloidal imprinting,[29] molecular imprinting,[30] etc. However all these techniques are limited to the production of thin films, and they use organic solvents, which have to be removed after the production process

In order to avoid all these disadvantages, the most promising technique in the production of bulk nanocellular polymers has been the gas dissolution foaming process, normally using CO_2 as blowing agent.

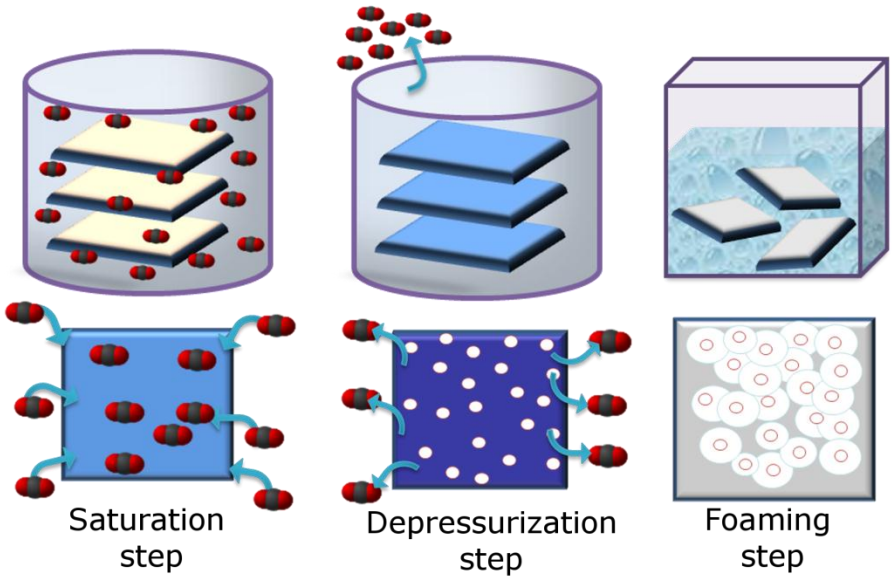

FIGURE 4. Gas dissolution foaming process scheme.

As it can be seen in Figure 4, this process consists of three steps. Saturation step, depressurization step and foaming step.

- Saturation step: The solid sample is introduced inside a pressure vessel under certain conditions of pressures and temperatures. Gas, normally CO_2, diffuses inside the sample, occupying the free volume that exists between the polymeric chains. After a certain time, depending on the saturation conditions and on the material, the sample becomes saturated, i.e. the sample contains the maximum amount of gas at the saturation conditions.
- Desorption step: Pressure is released, so after pressure release the sample is at atmospheric pressure. As a consequence the specimen is in a supersaturated state. When the sample is in supersaturated state gas behaves in two ways. On the one hand CO_2 starts to diffuse out of the sample. On the other hand, a phase separation between the gas phase and the polymer matrix phase take place, resulting in nucleation points.
- Foaming step: The presence of gas inside the polymer involves a reduction of the glass transition temperature of the material. Gas molecules dissolved inside the polymer matrix give some extra mobility to polymer chains giving as a result a reduction of this

characteristic temperature; this effect is known as plasticization effect. The new T_g is usually called effective glass transition temperature (T_{geff}). So in the last step, the sample is foamed in a thermal bath at a temperature higher than the $T_{geff.}$ At this moment, nucleation points have enough energy to grow into cells. This growth results in a macroscopic expansion of the sample and therefore in a density reduction.

2.2.2.2 Process parameters affecting the cellular structure

As it has been said previously, nanocellular materials presents high cell nucleation densities as well as low cell sizes, so in order to achieve these structures the mechanism of cells generation as well as the mechanisms controlling the cell growth have to be controlled.

Mechanisms of cell generation

As it has been explained previously, cells grow from nucleation points generated when the sample is under a supersaturated state. Two different nucleation mechanisms can be distinguished, homogeneous and heterogeneous nucleation.

Heterogeneous nucleation takes place in materials with different phases, one of them is the polymeric phase and the other can be impurities, nucleation agents, a second polymeric phase, etc. These pre-existing particles act as nucleation sites. In these materials the nucleation mechanism is controlled by parameters such as the amount of particles, the quality of the dispersion of the particles into the polymeric matrix, etc., and then, the influence of the process parameters is of less importance. On the other hand **homogeneous nucleation** takes place in pure materials, without any impurity. Homogeneous nucleation theory, developed by Colton and Suh,[31,32] provides an expression for the nucleation rate N_{hom} as shows Equation 6:

$$N_0 = Cf exp\left(-\frac{\Delta G}{k_B T}\right) \qquad [6]$$

Where Cf express the number of gas molecules per unit volume, and ΔG is the Gibbs free energy barrier for homogeneous nucleation given by Equation 7:

$$\Delta G^* = \frac{16\pi\sigma^3}{3\Delta p^2} \qquad [7]$$

Where Δp is the pressure difference between gas cells and solid and σ is the surface tension.

As nanocellular materials should present a high density of nucleation points, the nucleation rate has to be maximized in order to obtain these types of structures. Taking into account previous equations this is translated in:

- The amount of gas uptake Cf has to be maximized. This amount is controlled by the saturation parameters, saturation pressure and saturation temperature. The amount of gas uptake by the polymeric matrix depends on the pressure in different ways depending on the polymer. There exist three usual behaviors, given by Henry law, Langmuir Law and Dual law (Figure 5). [33]

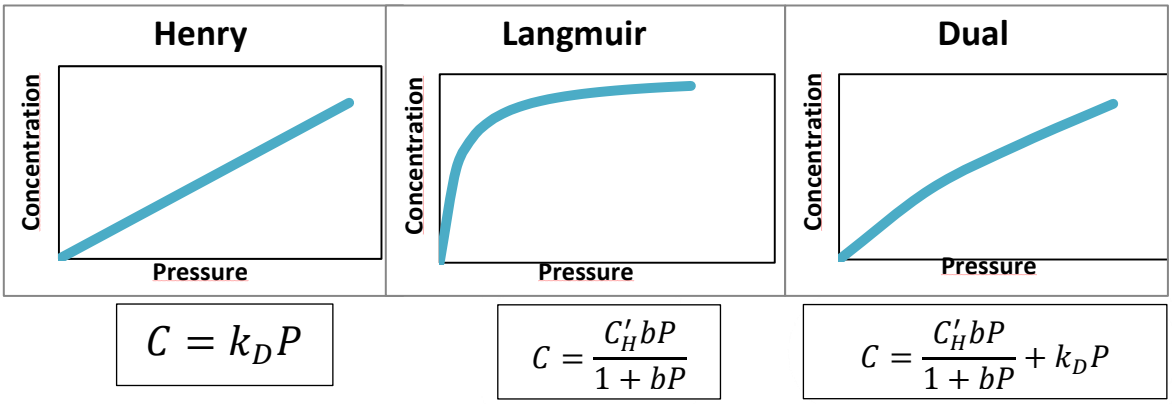

FIGURE 5. Laws governing the gas concentration dependence with saturation pressure.

Although each material behaves different under gas pressure, it is sure that the amount of gas uptake increases with the saturation pressure, so **saturation pressure has to be as high as possible.**

- The amount of gas uptake also depends on the saturation temperature. The solubility as a constant pressure process is given by Van´t Hoff law [34]:

$$S = S_0 \exp\left(-\frac{\Delta H_s}{RT}\right) \qquad [8]$$

Where ΔH_s is the enthalpy of sorption and depends on the material. CO_2-philic materials, such as PMMA, present a negative value of Helmholtz energy, so for them, solubility increases when temperature decreases, for these reason **saturation temperature has to be as small as possible.**

- Finally other essential parameters are the pressure drop and the depressurization ratio; higher pressure drop and pressure drop rates produce higher thermodynamic instability and therefore a higher probability of nucleus formation. **For this reason pressure drop and depressurization rate should be maximized.**

Mechanisms of cell growth

In order to obtain cell growth it is necessary to increase the temperature of the polymer above its effective glass transition, so in this step is really important to control the foaming temperature as

well as the foaming time. These two parameters have to be sufficiently high to allow the totally expansion of the structure but not too high, because in that case some degeneration mechanisms of the cellular structure, such as coalescence, drainage or coarsening, will appear. **So in foaming step foaming time and foaming temperature have to be optimized for each material.**

3 Objectives

As it was previously mentioned there exist different strategies for the production of nanocellular materials. On the one hand, they can be produced by acting on the process parameters as well as by acting on the process itself. On the other hand, by adding nanoparticles acting as nucleation sites or by using nano-structured polymers to obtain an heterogeneous nucleation mechanisms. This investigation is focused on the first of them; the fabrication of improved nanocellular materials by means of the optimization of the process parameters using a pure polymer in which nucleation is homogeneous.

Up to date nanocellular materials produced from pure PMMA present relative densities in the range of 0.3 to 0.6. So the aim of this study is working in the process in order to find the conditions that lead to lower densities materials.

The main objectives of the master thesis are:

- The study and optimization of the process parameters of the gas dissolution foaming process with the aim of producing low relative densities materials using an homopolymer (PMMA) as raw material.
- To perform a detailed analysis of the descriptors defining the cellular structure; both in the solid phase as well as in the gaseous phase, in order to obtain the process-density-cellular structure relationship for these novel materials.

4 Experimental

4.1 Materials

Polymethylmethacrylate (PMMA) V 825T was kindly supplied by ALTUGLAS® International in the form of pellets. PMMA is a transparent thermoplastic which repeating unit is shown in Figure 6. This material has been widely used as an alternative to glass thanks to its properties; it is a strong and lightweight material, it presents good impact strength, and also it is almost transparent. These properties, among others, make this polymer a good candidate for the fabrication of polymeric foams. The material used presents a density (ρ) of 1.19 g/cm^3 (measured at 23ºC and 50%RH) and a glass transition temperature (T_g) of 114.5^{o}C measured by DSC. Medical grade CO_2 (99.9% purity) was used as blowing agent.

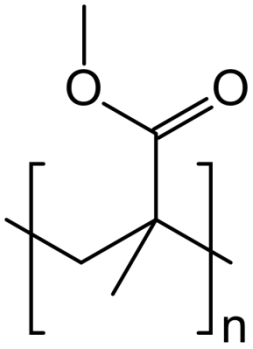

FIGURE 6. Repeating unit of Poly(methylmethacrylate)

4.2 Precursors production

The polymer was processed into sheets of (155x75x4 mm^3), using a cold/hot plate press. A steel mould has been used in order to obtain precursors of the desired dimensions. The process consists of three steps. First of all, the pellets of the raw material (Figure 7.a) were heated during 9 minutes at 250ºC, without applying any pressure.

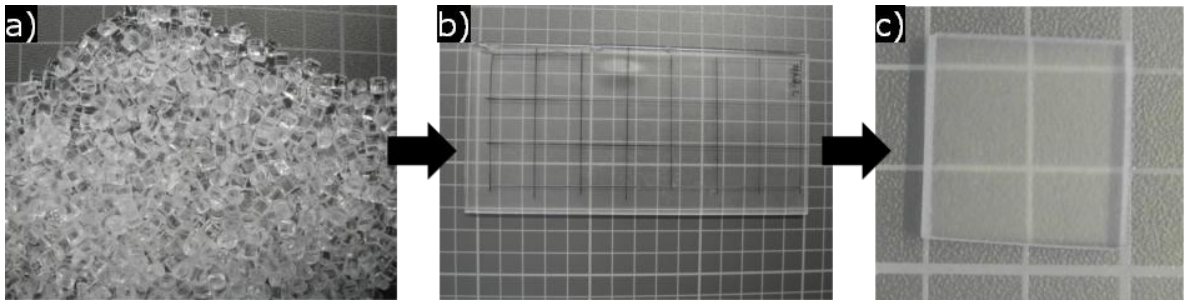

FIGURE 7. Precursor's production route.

This temperature is higher than the glass transition temperature of the polymer in order to achieve a high mobility that allows the polymer to be thermoformed. In the second step, the material is pressed under a constant pressure of 2.2 MPa for one minute in order to thermoform it with the shape of the mould. Finally, precursors were cooled down to room temperature in the cold plates during 4 minutes and under the same pressure (2.2MPa). These sheets (Figure 7.b) were later cut into 20x20x4 mm^3 samples in order to use them for foaming experiments (Figure 7.c).

4.3 Cellular materials production

Foaming experiments were performed in a high pressure vessel (model PARR 4681) provided by Parr Instrument Company. The system to supply the gas pressure comprises an accurate pressure pump controller (model SFT-10) provided by Supercritical Fluid Technologies Inc. Thermal baths (J.P. Selecta Model 6000685) have been used to heat the samples after saturation with CO_2. All this set-up, shown in Figure 8, has been used in order to carry out the gas dissolution process in different samples. As it has been said, this production route consists of three stages, the saturation step, the desorption step and the foaming step. Samples are introduced in the pressure vessel under a high pressure atmosphere, achieved through the pressure pump, up to saturation. Then the pressure is released by means of the electrovalve and finally samples are immersed in a thermal bath for foaming (Figure 8.c), obtaining the final sample (Figure 9.b)

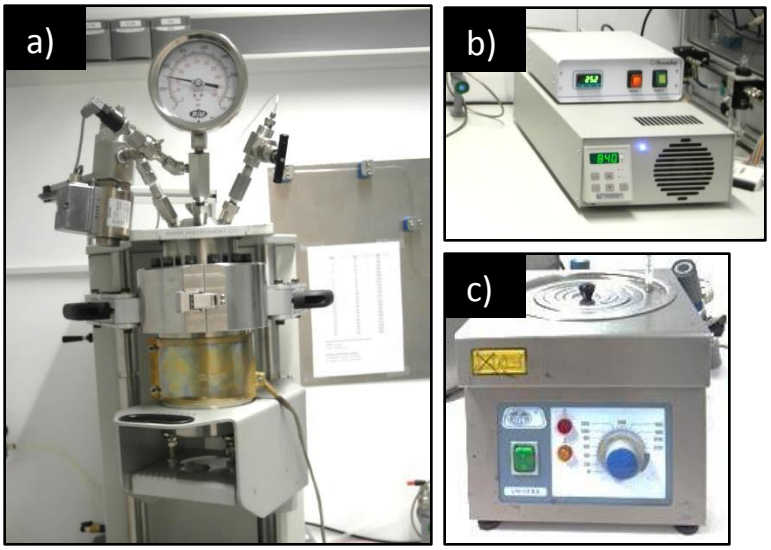

FIGURE 8. Set up for the nanocellular samples production.**(a)** Pressure vessel. **(b)** Temperature and pressure controllers. **(c)** Thermal bath.

In this study, a set of samples has been produced varying the production parameters. Saturation and depressurization parameters have been fixed for all the samples according to the literature, in order to obtain a high cell nucleation density. Saturation parameters have been chosen to achieve a 31% of CO_2 uptake, amount suitable to produce nanocellular materials in PMMA.[1,35] Saturation

pressure (p_{sat}) was fixed at 31 MPa and saturation temperature (T_{sat}) at 25ºC. Saturation time was 24h for all the experiments, enough time to reach saturation. After saturation, the pressure was released using a fast depressurization rate of 100MPa/s that has been achieved thanks to an electrovalve with Kv = 1.1 l/min. Desorption time (time between the depressurization and the immersion of the samples in thermal baths) was fixed in three minutes for all the experiments. Foaming temperatures have been modified from 40ºC to 110ºC and foaming times from 1 minute to 5 minutes in order to study the influence of these parameters in the density and cellular structure.

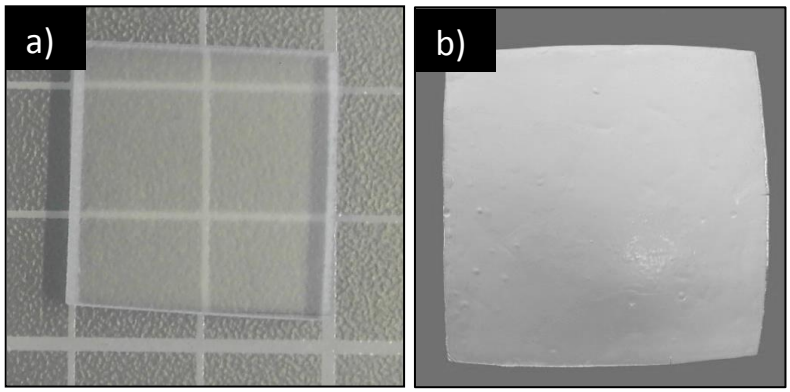

FIGURE 9. **a)** Original sample. **(b)** Foamed sample.

4.4 Characterization techniques

In order to characterize the solid material as well as the cellular materials produced, different characterization techniques have been used:

Amount of gas uptake

In order to determine the total amount of CO_2 uptake by PMMA a Mettler-Toledo balance has been used. The expression used is shown in Equation 9:

$$CO_2 uptake\ (\%wt) = \frac{m_f - m_0}{m_0}\ 100 \qquad [9]$$

Where m_0 is the initial mass of the sample and was measured before the experiment and m_f is the mass of the sample after full saturation. There exists a temporal gap between the depressurization and the weighed of the sample, so in order to determine accurately the total amount of gas uptake the loss of mass as a function of time was registered with the balance. Then, taking into account the initial part of this function (linear behavior) an extrapolation to zero desorption time was performed to obtain a more accurate value of m_0 (Figure 10).

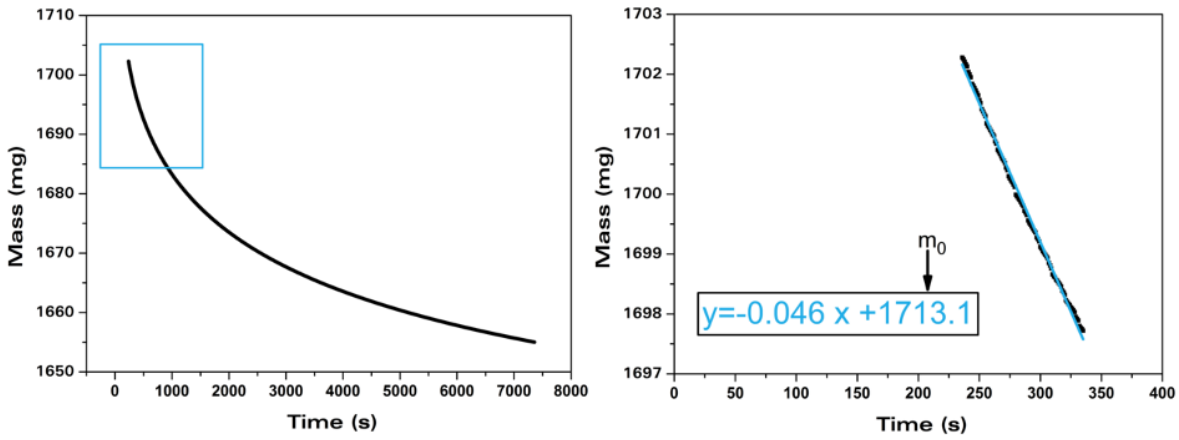

FIGURE 10. (**a**) Mass loss of a sample after the depressurization. (**b**) Linear behaviour of mass loss after the depressurization.

As it can be observed the correction introduced by this calculation is small due to the small diffusivity of CO_2 in this material.

Density

Density of solid precursors has been determined by means of a gas pycnometer (Mod. AccuPyc II 1340, Micromeritics). Density of cellular polymers produced has been measured, three times for each specimen, using the water-displacement method, based on Archimedes' principle. A density determination kit for a Mettler-Toledo balance (Mod.AT261) has been used for this purpose.

Open Cell Content

The percentage of open cells (OC %) was measured with a gas pycnometer (Mod. AccuPyc II 1340, Micromeritics), according to ASTM D6226-10. The equation to calculate the open cell content is:

$$O_v(\%) = \frac{V - V_p - V_s}{V(1 - \rho_r)} \qquad [10]$$

Where V is the geometric volume of the sample, V_p is the volume measured by the pycnometer and Vs takes into account the exposed cells at the surface of the sample. The external volume V, has been determined from the cellular material density (measured by the water-displacement method) and its mass (m) (measured with an AT261 Mettler- Toledo balance) as $V = m/\rho$. In order to determine V_p a pressure scan (from 0.2MPa to 1.3MPa) with a gas pycnometer has been performed measuring the pycnometric volume for each pressure. From a certain pressure this value of volume remains constant, which demonstrate that no more gas can enter inside the cellular material. V_p has been considered as the mean value of these last constant values measured as Figure 11 shows:

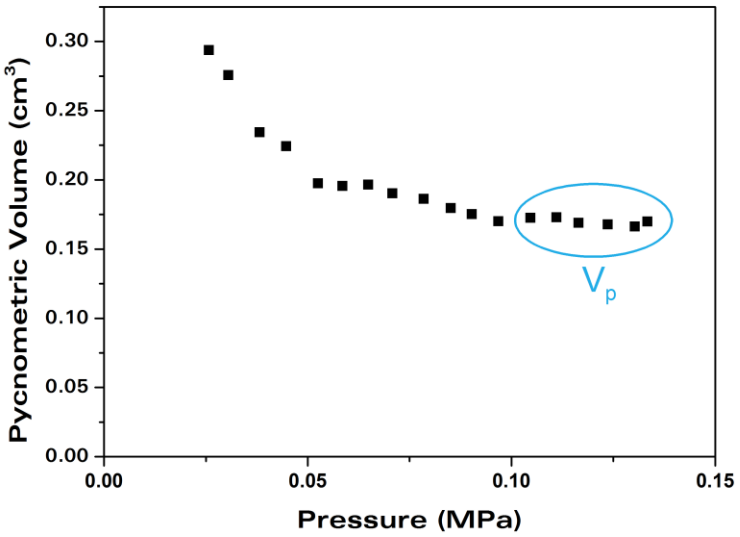

FIGURE 11. Pycnometric volume measured as a function of pressure. The constant values obtained at high pressure were used to calculate the open cell content in the samples.

As V_s is proportional to the cell size, this value becomes negligible for nanocellular materials and due to this it was not included in equation 10.

Scanning electron microscopy

SEM micrographs have been used in order to characterize the parameters of the cellular structure defined previously, of each specimen. In order to obtain these micrographs, nanocellular materials have been prepared for the visualization. First of all, samples were cooled in liquid nitrogen and then fractured in order to preserve the original structure. Then samples were coated with gold by means of a sputter coater (model SDC 005, Balzers Union). An ESEM Scanning Electron Microscope (QUANTA 200 FEG) has been used to obtain the micrographs.

In order to analyse the cellular structure, software based on ImageJ/FIJI [36] has been used. This software provides information about, cell size (ϕ), cell size distribution, standard deviation of the cell size distribution (SD), anisotropy ratio (AR), cell density N_v and cell nucleation density N_0. A total of two micrographs randomly obtained have been used for the analysis of each material. Therefore, more than 300 cells have been considered for each specimen.

As it has been mentioned, there exist some advanced descriptors of the cellular structure that have been also measured in this study, as the mean cell wall thickness or the fraction of mass in the struts.

The mean cell wall thickness has been measured directly from the micrographs, as it is shown in Figure 12. In these 2D images it is also possible to distinguish between cell walls (ξ) and struts (S).

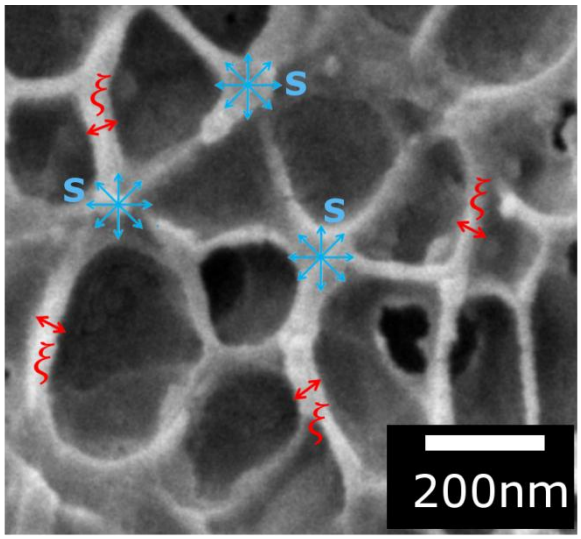

Figure 12. SEM micrograph showing the different parts of the solid phase in a cellular material, cell walls (ξ) and struts (S).

More than sixty cell walls have been measured from each sample. The final value of cell wall has been the average value of all these measurement. It has to keep in mind that this is a 2D characterization method so broken walls cannot be measured with this method. It means that the measured mean cell wall thickness values correspond to visible, i.e. non-broken, cell walls.

In order to determine the fraction of mass in the struts different steps have been followed using ImageJ/FIJI. The whole process is illustrated in Figure 13.

First of all, a representative region of the original SEM micrograph was cropped, then cells were marked creating a mask as it can be seen in Figure 13.a. Then a binarized image was created, separating the solid phase, marked in white, and the gaseous phase, marked in black. This image can be seen in Figure 13.b. As it can be seen the two phases are now clearly differentiated. Now it is possible to use the local thickness tool of ImageJ/FIJI. This tool sets up a colour map assigning a different colour for each different thickness as it can be seen in Figure 13.c. In this local thickness image it is easy to distinguish between struts, thicker parts, and walls, thinner parts. Finally a histogram was obtained from this local thickness image, shown in Figure 13.d, the histogram quantifies the relative frequency corresponding to each thickness. Low values of thickness correspond to cell walls and high values of thickness correspond to struts. It means that in the histogram there exist two different distributions one for cell walls and the other one for struts. In order to separate these two distributions a threshold value has been chosen to be the minimum thickness value corresponding to a strut, or in other words the maximum thickness value corresponding to a cell wall. This thickness was chosen by measuring the different struts in the corresponding image and selecting the minimum value as the threshold value. As it can be seen in the histogram this allows to differentiate the two different distributions. Finally the fraction of mass in the struts, f_s can be determined as the sum of relative frequencies corresponding to the struts distribution. Some samples (those with lower densities) did not present sufficient

differences in thickness between cell walls and struts, so for these particular samples it was not possible to apply this method of quantification.

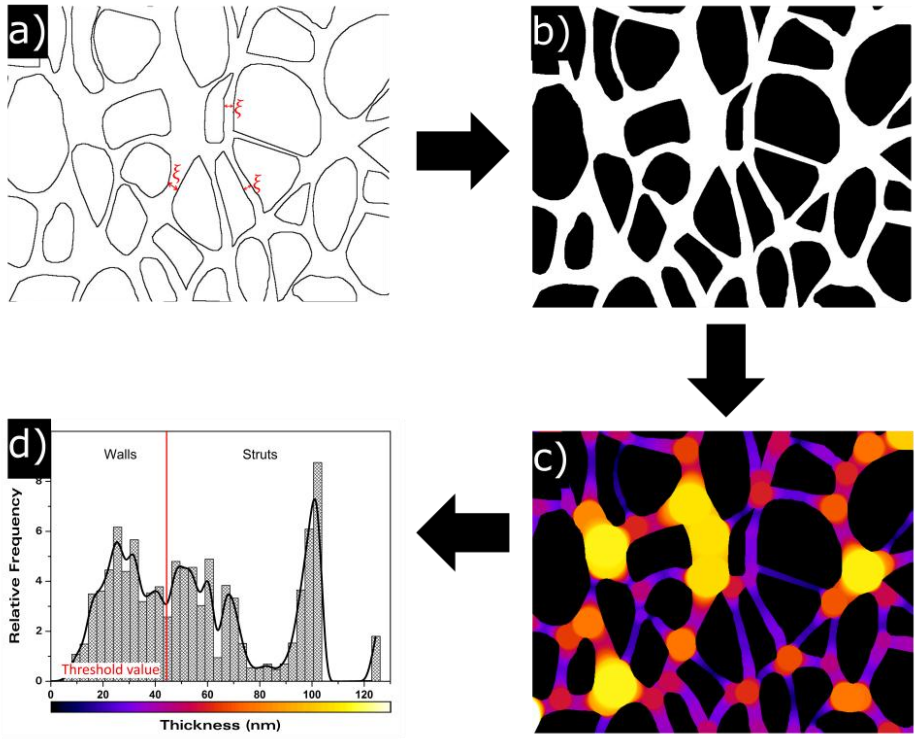

FIGURE 13. Description of the method to measure the fraction of mass in the struts (f_s).

Differential scanning calorimetry (DSC)

Glass transition temperature of the solid and foamed samples has been measured by means of a Mettler DSC30 differential-scanning calorimeter previously calibrated with indium.

Glass transition temperature is calculated as the mid-point of the drop in the DSC thermogram that characterizes this transition. The DSC was prepared with the same amount of mass for each sample, approximately 5mg. The measurement process comprises three steps, first of all a first heating step was performed between 20ºC and 160ºC at 10ºC/min, in order to determine the T_g of the processed samples. Then the thermal history of the samples were erased by maintained them at 160ºC during 3 minutes and then cooled them down from 160ºC to 20º at -10ºC/min. Finally the initial heating step was repeated to determine the T_g of the sample after erasing of the thermal history.

This experiment was performed in both, solid and foamed samples. This way the T_g increment (ΔT_g) can be defined as the difference between the glass transition temperature, measured in the first heating step, of the cellular material and the glass transition temperature determined in the first heating step, of the solid one. The same quantification was performed for the glass transition temperature measured in the second heating step defining ΔT_{g_2}.

5 Results

5.1 Influence of the foaming parameters

A set of 24 samples have been fabricated by gas dissolution foaming process. In order to study the influence of foaming temperature and time in the final cellular structure, saturation and desorption parameters were fixed and the foaming conditions were modified. Foaming temperature has been varied from 40 ºC to 110 ºC increasing in intervals of 10 ºC. Moreover three different times have been studied for each foaming temperature, 1 minute, 2 minutes and 5 minutes. The different characteristics of all these samples are shown in Table 1, and will be discussed in the following paragraphs. The section is divided in two different parts. First, the study of the gaseous phase is presented and then, the study of the solid phase of the cellular structure is discussed.

Sample	F.Time (s)	F.Temp. (ºC)	ρ_r	N_0 (1/cm^3)	Φ (nm)	SD/ϕ	AR	ξ (nm)	f_s	OC (%)	ΔT_g (ºC)	ΔT_{g2} (ºC)
1	1	40	0.47	$1.78\ 10^{14}$	212	0.45	1.24	26	0.60	4	4.9	0.1
2	2	40	0.43	$1.55\ 10^{14}$	220	0.37	1.22	30	0.54	3	6.4	2.1
3	5	40	0.37	$2.17\ 10^{14}$	225	0.39	1.26	24	0.54	8	7.3	0.7
4	1	50	0.42	$1.74\ 10^{14}$	219	0.40	1.30	24	0.57	4	5.9	-0.5
5	2	50	0.37	$2.24\ 10^{14}$	213	0.41	1.32	26	0.47	4	8.5	0.8
6	5	50	0.32	$2.16\ 10^{14}$	241	0.41	1.27	24	0.54	21	9.9	0.3
7	1	60	0.39	$2.38\ 10^{14}$	207	0.42	1.21	26	0.46	5	8.3	1.6
8	2	60	0.33	$2.34\ 10^{14}$	221	0.40	1.27	26	0.36	11	10.0	-0.7
9	5	60	0.29	$2.12\ 10^{14}$	236	0.47	1.26	23	0.38	30	9.6	1.4
10	1	70	0.35	$2.27\ 10^{14}$	221	0.44	1.24	24	0.39	12	7.8	1.2
11	2	70	0.28	$2.19\ 10^{14}$	229	0.46	1.20	30	0.36	47	10.5	1.5
12	5	70	0.27	$2.73\ 10^{14}$	221	0.44	1.28	25	0.34	73	10.3	0.3
13	1	80	0.27	$3.56\ 10^{14}$	208	0.45	1.21	23	0.35	73	10.5	0.7
14	2	80	0.26	$3.15\ 10^{14}$	227	0.40	1.14	26		90	10.6	2.2
15	5	80	0.29	$2.81\ 10^{14}$	224	0.41	1.23	29	0.35	91	11.3	2.4
16	1	90	0.27	$3.04\ 10^{14}$	222	0.40	1.12	29	0.35	99	10.0	0.5
17	2	90	0.26	$3.13\ 10^{14}$	222	0.44	1.14	26		100	10.3	1.0
18	5	90	0.26	$2.79\ 10^{14}$	234	0.40	1.09	28		100	10.5	0.6
19	1	100	0.27	$3.44\ 10^{14}$	204	0.41	1.18	28	0.31	100	10.9	1.9
20	2	100	0.24	$3.60\ 10^{14}$	216	0.46	1.03	26		97	10.7	2.5

21	5	100	0.28	2.67 10^{14}	234	0.43	1.16	29	0.31	100	11.4	1.1
22	1	110	0.25	2.23 10^{14}	261	0.43	1.19	28		99	11.0	1.4
23	2	110	0.27	2.99 10^{14}	227	0.43	1.04	33	0.32	100	10.9	1.0
24	5	110	0.37	3.10 10^{14}	184	0.40	1.17	36	0.54	46	4.5	2.0

5.1.1 Gaseous Phase

Relative density

In order to determine how evolves the relative density with the foaming parameters, this value has been measured for all the samples. Then the evolution of relative density with the foaming temperature as well as with the foaming time has been studied, as can be seen in Figure 14.

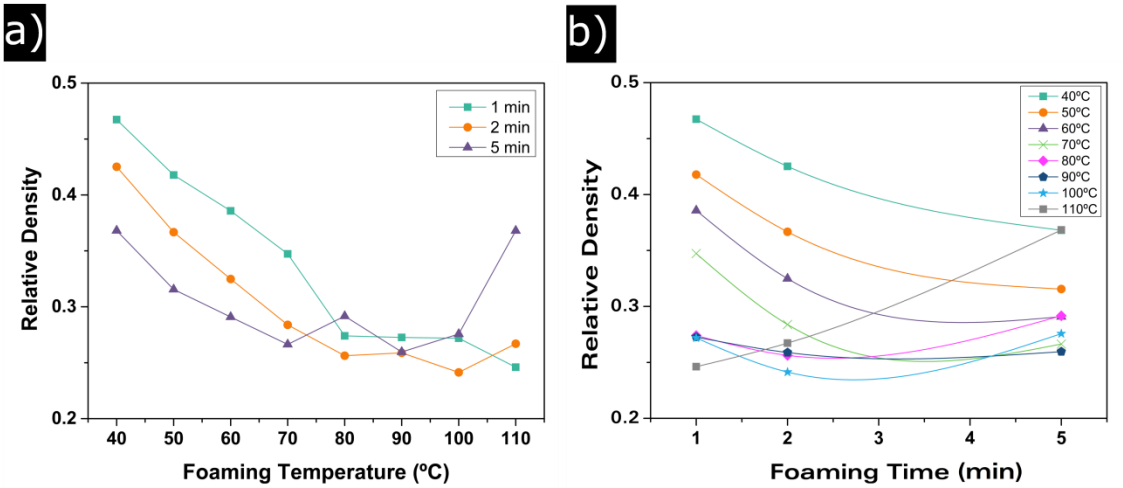

FIGURE 14. (**a**) Relative density evolution as a function of foaming temperature; (**b**) Relative density evolution as a function of foaming time.

In Figure 14.a it can be seen that up to 80ºC an increase in the foaming temperature results in a decrease in the relative density. From 80ºC to 100ºC relative density remains almost constant with the foaming temperature. This is also true for samples foamed at 110ºC during 1 and 2 minutes, but at 5 minutes of foaming time the relative density increases again. On the other hand, in Figure 14.b the evolution of relative density with the foaming time can be analyzed. An increase in the foaming time results also in a decrease of the foaming temperature up to temperatures of 80ºC. From 80ºC to 100ºC similar values of relative density are observed for all the foaming times. Once again, it can be seen that relative density curve that corresponds to 110ºC of foaming temperature do not follow the general trend; the minimum value of relative density is reached at one minute of foaming time and then the density raises up to 0.35 for 5 minutes of foaming time.

It can be concluded that cellular materials presenting different relative densities values can be obtained by varying the foaming conditions. For these saturation conditions, the minimum relative

density that can be reached is 0.25 and can be obtained by maintaining the foaming temperatures above 80ºC and below 110ºC and the foaming times in the range from 1 to 5 minutes. It can be also concluded that 110ºC is the upper limit at which materials with low relative densities can be produced.

Cellular structure

Cellular structure of all samples has been analyzed by means of micrographs obtained by SEM. Some of these micrographs are shown in Figure 15.

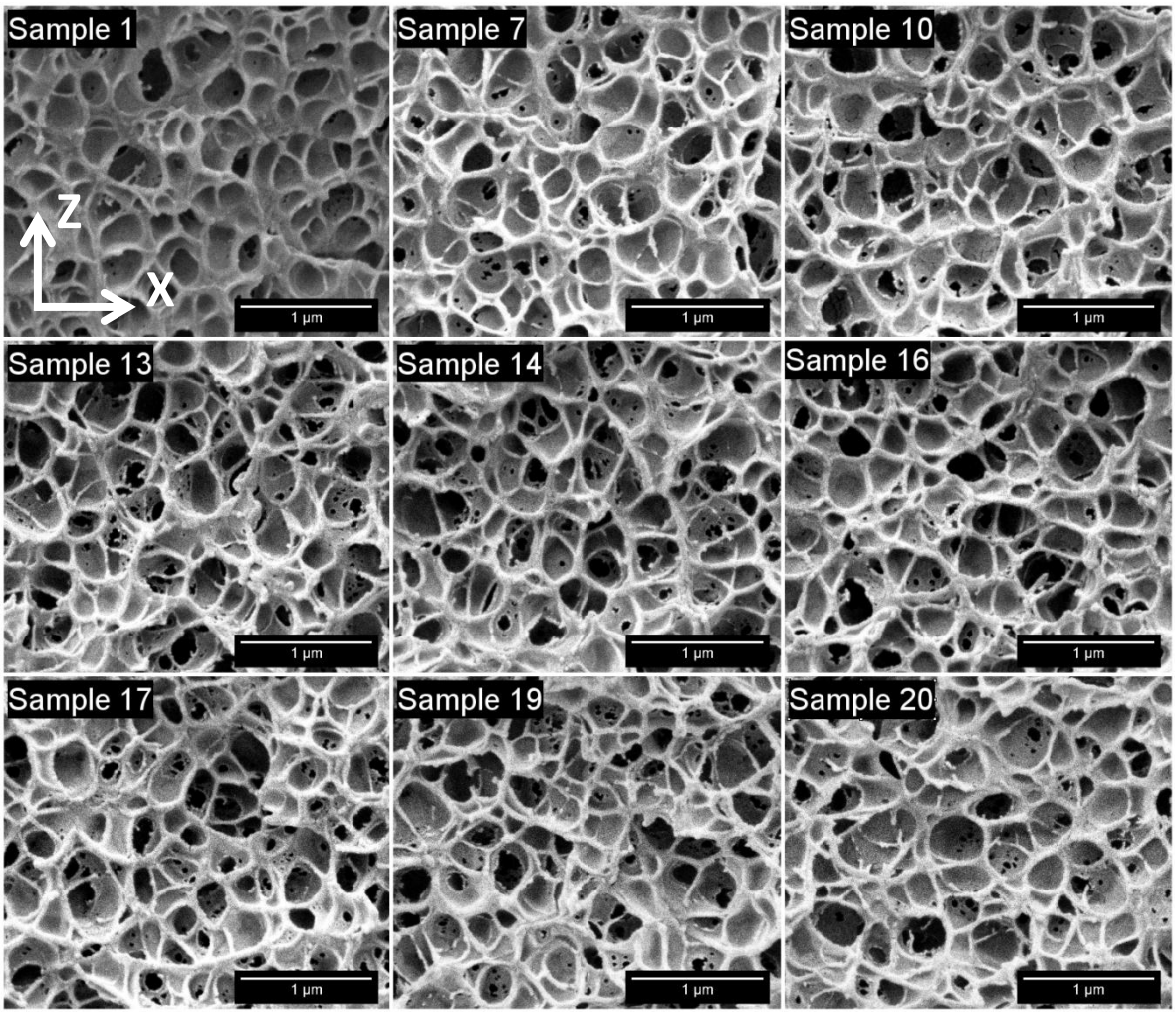

Figure 15. Micrographs of some selected samples.

As it can be seen, with a naked eye, samples present cell sizes in the nanometric range. It can be also observed the high homogeneity of the cellular structure, and a small anisotropy in direction Z (Figure 15) that corresponds to the compression direction during the production of the solid precursor. All the parameters that define the cellular structure have been measured, and the results will be discussed in the following paragraphs.

The evolution of the cell size as well as the cell nucleation density with the foaming parameters is shown in Figure 16.

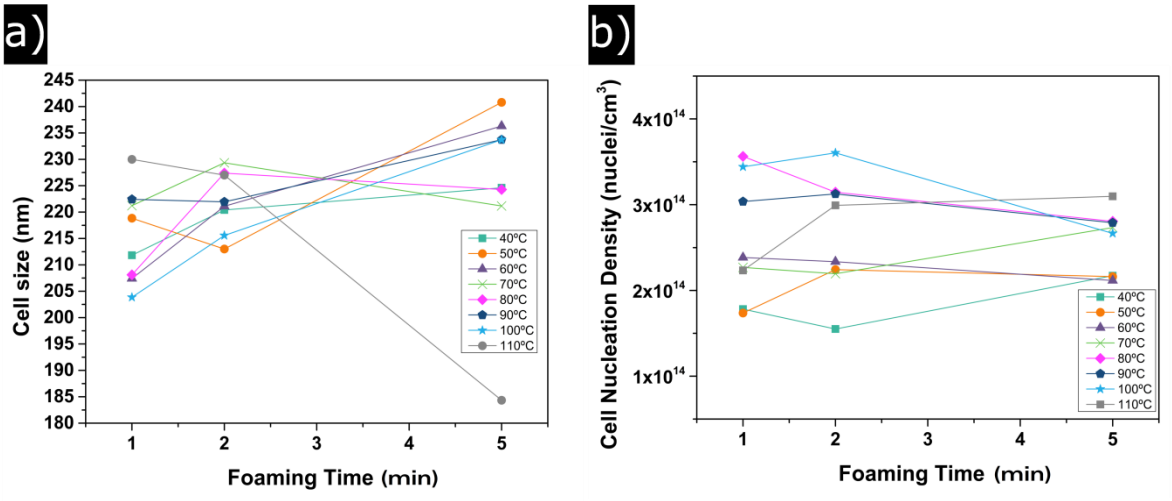

Figure 16. (**a**) Evolution of the cell size with foaming time; (**b**) Evolution of cell nucleation density with foaming time.

If the general trend is observed, foaming time produces a small increase in cell size (Figure 16.a), from 205 nm at 40ºC to 240 nm at 100ºC. Nevertheless, this is a really small change, so it can be said that all samples present constant cell sizes in the nanometric range of around 200 nm. 110ºC of foaming temperature follows the general trend for 1 and 2 minutes of foaming time, but, as it has been previously observed, at 5 minutes of foaming time, cell size is reduced due to the collapse of the cellular structure at these foaming conditions. In order to prove that all samples present homogeneous cellular structures SD/Φ has been determined, the value for each sample is shown in Table 1. The ratio remains constant with foaming time as well as with foaming temperature, with a value near 0.4. This value indicates that all samples are very homogeneous, so it can be concluded that for these saturation conditions the homogeneity of the cellular structure does not depend on the foaming conditions.

When the cell nucleation density is studied (Figure 16.b) two groups can be clearly differentiated. On the one hand samples produced at foaming temperatures from 40ºC to 70ºC present cell nucleation densities of around $2 \cdot 10^{14}$, while samples foamed from 80ºC to 110ºC present cell nucleation densities higher than $3 \cdot 10^{14}$.

Open Cell Content

The evolution of the open cell content with the foaming temperature has been also studied as it is shown in Figure 17.

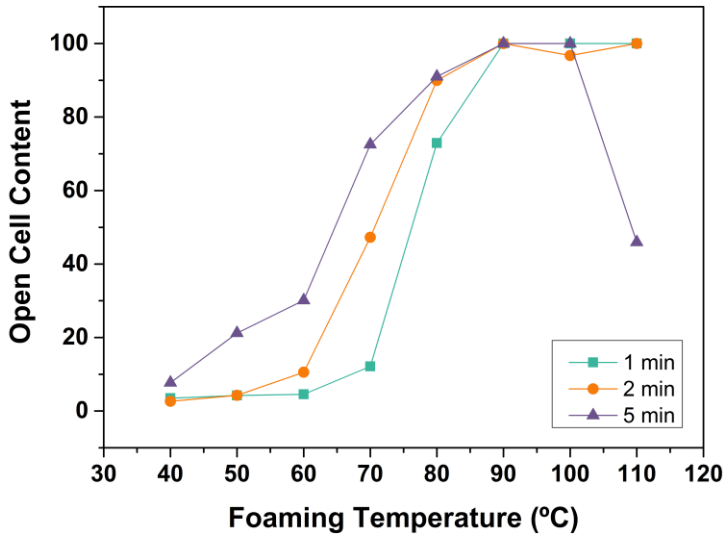

Figure 17. Evolution of the Open Cell Content with the foaming temperature.

The evolution of this magnitude with the foaming parameters is clear; up to 90ºC of foaming temperature, OC increases as foaming temperature increases, while 90ºC, 100ºC and 110ºC produce totally open cell materials. Also, it is visible that foaming time increases the open cell content; 5 minutes of foaming time produces a higher amount of open cells than 1 minute. As has been observed, sample produced at 110ºC and 5 minutes does not follow the general trend; it presents a lower value of OC due to the collapse of the cellular structure.

5.1.1.1 Discussion

Cellular structure

Up to this point it has been studied how the gaseous phase of cellular structure changes with respect to the foaming parameters. Also it has been described how relative density evolves with these parameters. So in this section the materials density and the changes in the gaseous phase are correlated.

As it has previously seen the two principal parameters that define the gaseous phase are the cell size and the cell nucleation density. So these two parameters will be first analyzed.

As mentioned above relative density changes from 0.47 for sample 1, material with the highest density, to 0.24 for sample 20, material with the lowest one (Figure 14). It means that relative density changes by a factor two between sample 1 and sample 20.

It might be think that this change in relative density is due to an increase in the cell sizes between these two samples. But, if it is consider that the number of cells is constant, a change in a factor two in relative density should be translated in a change in a factor 1.26 ($2^{1/3}$) in the cell size. As it can be determined the ratio of cell sizes between samples 1 and 20 is only 1.02. It means that the significant change observed in the relative density cannot be caused by an increase in the cell size.

Of course, the comparison between these two samples is only an example of the general trend observed in all the samples under study as it can be seen in Figure 18.

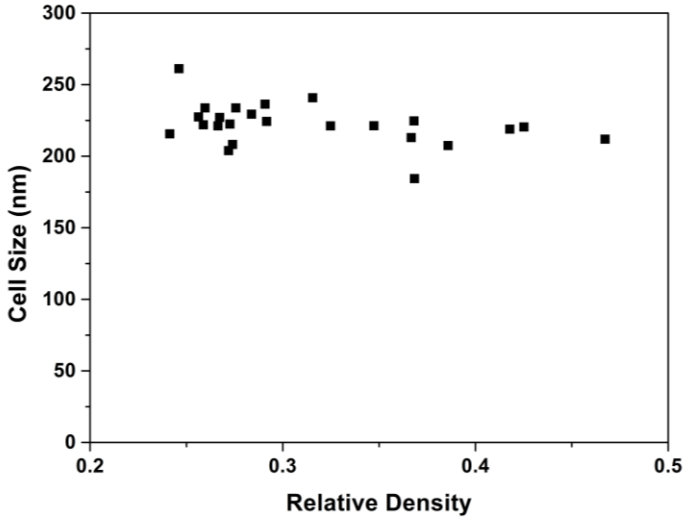

Figure 18. Evolution of the cell size with the relative density.

There is no a clear trend when the change in the cell size is observed with respect to the relative density so, in spite of the relative density evolution the cell size can be considered constant in the range of our study.

Therefore, we need to analyze in detail the cell nucleation density. As it can be seen this magnitude evolves with the foaming parameters, from 1.5 10^{14} nuclei/cm^3 for samples produced at 40ºC of foaming temperature to 3.5 10^{14} nuclei/cm^3 for samples produced at higher temperatures (Figure 19.a).

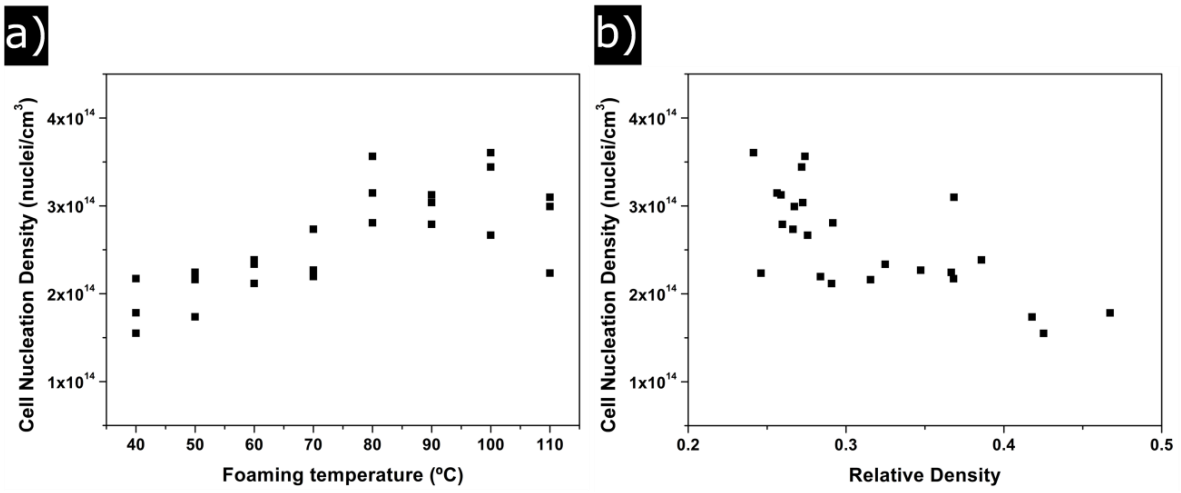

Figure 19. (**a**) Evolution of the Cell nucleation density with foaming temperature; (**b**) Evolution of cell nucleation density with relative density.

It means that N_0 doubles its value between samples of higher relative densities and samples with lower ones.

Figure 19.b shows that cell nucleation density increases as relative density decreases. It means that samples with lower density values present twice cells than samples presenting higher values of relative density.

As a conclusion, the change in relative density that was found by changing the foaming conditions is mainly due to the high number of cells that appear when temperature is increased.

Open cell content

In the previous section, it was shown that open cell content evolves significantly with the foaming conditions. The relationship between OC and the relative density has been also studied. As it can be seen in Figure 20, there exists a clear correlation between the two magnitudes. Samples with high relative densities present low contents of open cells, i.e. it doesn't exist interconnectivity between the cells. As density decreases, by changing the foaming conditions the interconnectivity between cells increases up to a maximum value of 100%. It means that samples presenting lower values of density have a totally interconnected gas phase.

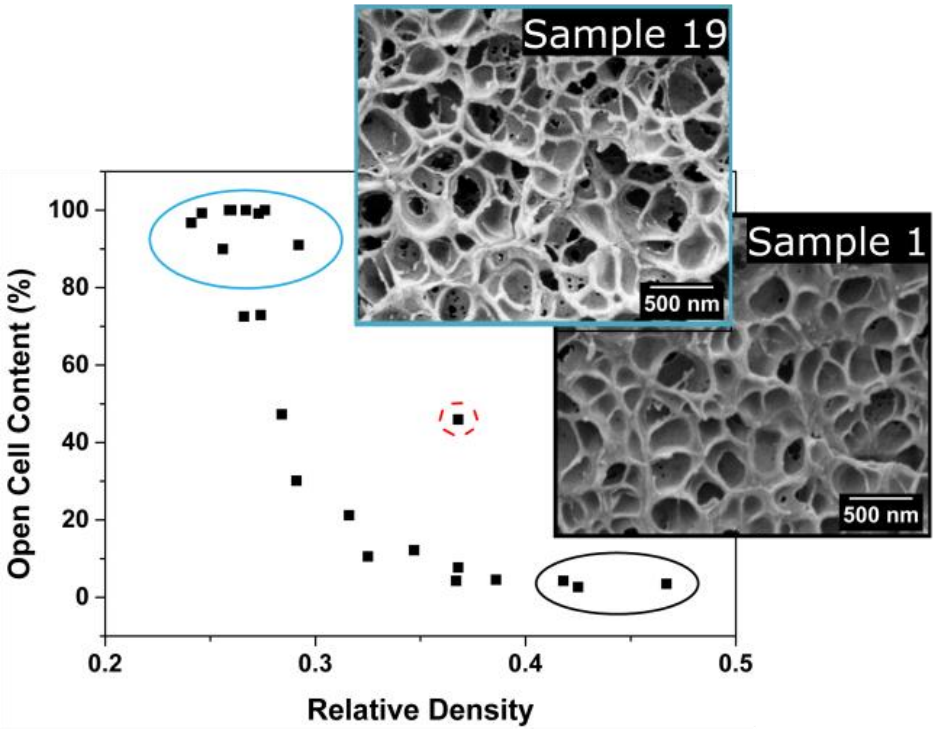

Figure 20. Open Cell content as a function of relative density.

This evolution is clearly observed in the SEM micrographs. In Figure 20 it can be seen a clear tendency of the open cell content with the relative density, samples with a high relative density

(circled in black) present a closed structure while as relative density is reduced cellular structure become open. At this way samples with lower relative densities present totally open cellular structures (circled in blue). Moreover two micrographs are shown in figure 20; sample 1, with a relative density of 0.47 has closed cells. On the other hand sample 19 with a value of relative density of 0.27 presents a high interconnectivity between cells, and the measured value of OC was 100%. Figure 15 showed how the cells structure becomes open with the reduction of the density, up to reaching the total connectivity for values of relative densities lower than 0.27.

As previously discussed, samples with the lowest relatives densities were producing with high foaming temperatures, these temperatures decrease the polymer viscosity inducing the rupture of cell walls during the expansion process. On the other hand, as it will be discussed in the next section, cell wall thickness measured is constant with the foaming conditions, it means that there must be a minimum thickness value below which cell walls break, and this value seems to be round 23nm.

It is also interesting to point out that the sample produced at 110ºC and 5 minutes (circled in red in Figure 20) do not follow the trend of the other materials. It has a higher open cell content than those materials with similar densities. This is due to the fact that the cellular structure of this sample has suffered degeneration due to the high temperature and time used for their production.

5.1.2 Solid Phase

Anisotropy ratio

As it was previously said, other parameters have been measured in order to totally characterize the cellular structure. All of them can be seen in Table 1.

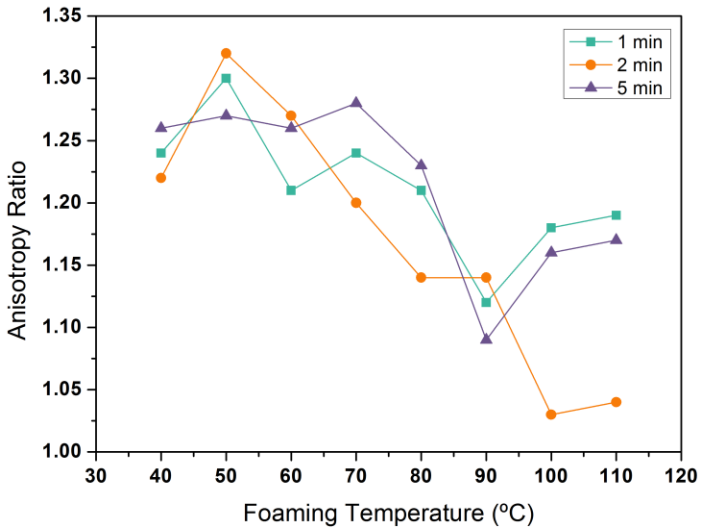

Figure 21. Evolution of the anisotropy ratio with foaming temperature.

First of all the anisotropy ratio can be observed to be higher than 1 for all the cellular materials (Figure 21). It means that as it could be seen in SEM images (Figure 15) cells are slightly elongated in Z direction, that is, the direction of the applied pressure during the solid precursor's production. However this anisotropy seems to be reduced with the foaming temperature, obtaining higher values for low foaming temperatures and low AR for higher temperatures. As it can be seen, for temperatures below 60ºC present AR around 1.2 and 1.3 while for samples produced at a foaming temperature higher than 60ºC the samples present an anisotropy ratio value between 1.0 and 1.2.

Cell wall thickness

Results concerning the cell wall thickness can be seen in Table 1 and in Figure 22, where it has been represented as a function of foaming temperature.

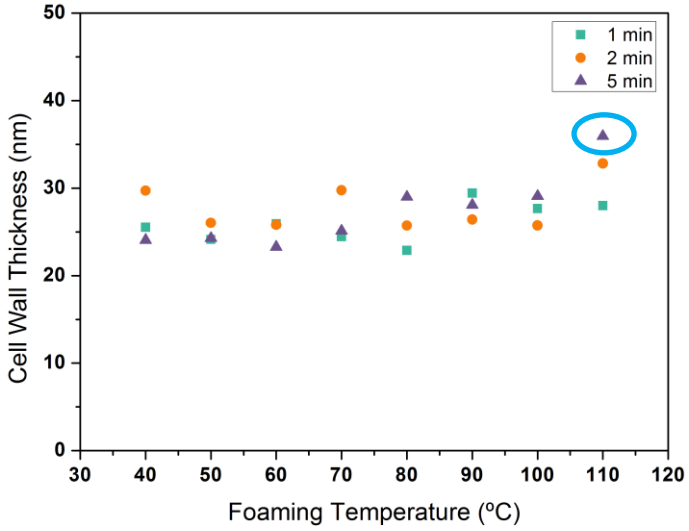

Figure 22. Cell wall thickness with respect to foaming temperature.

As it can be seen ξ hardly changes with foaming conditions, obtaining values between 23 nm and 30 nm no matter what the foaming conditions are. Sample produced at 110ºC and 5 minutes is enclosed in blue in Figure 22, and presents little higher values than the rest of the samples. As it has been previously commented the structure of this samples is collapsed so the cell size is smaller and the cell walls thicker.

Fraction of mass in the struts

Otherwise, fraction of mass in the struts evolves significantly with foaming conditions. As it can be seen in Table 1 and Figure 23, f_s changes from 0.6 for samples produced at lower foaming temperatures to 0.3 for sample produced at higher ones. This is true for all foaming times.

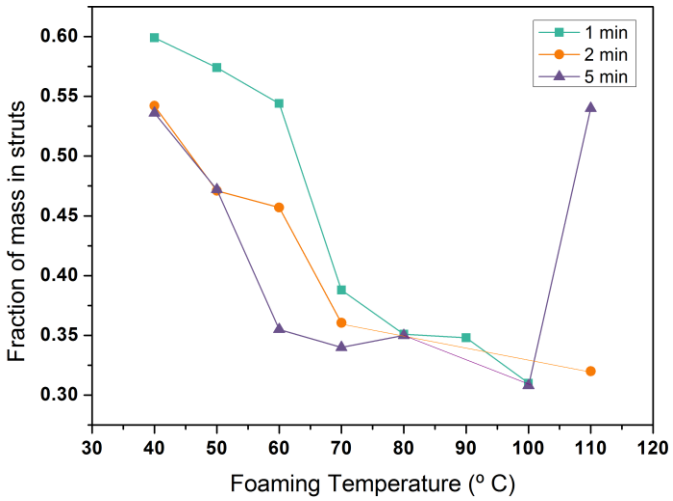

Figure 23. Fraction of mass in the struts with respect to foaming temperature.

So in conclusion fraction of mass in the struts decreases as foaming time increases. Of course, this is not true for sample 24 (110ºC / 5 min) in which due to its higher density the fraction of mass in struts increases.

5.1.2.1 Discussion

As well as the gaseous phase evolves with the foaming conditions, and this evolution was related with the changes in relative density, the same type of analysis is carried out in this section for the solid phase. Parameters such as the cell wall thickness and the fraction of mass in the struts are related with the changes in density.

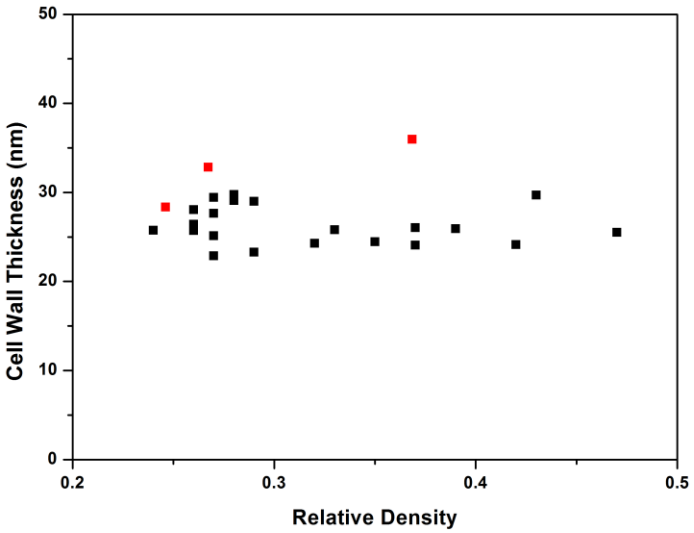

Figure 24. Cell wall thickness evolution with respect to relative density.

In the results section, it was found that the cell wall thickness (ξ) was constant in the range of studied relative densities, so this parameter does not present any tendency with the relative density (Figure 24). Samples foamed at 110ºC are marked in red in order to clearly seen that from 2 minutes of foaming they are above the general trend, presenting thicker cell walls.

So, with respect to the solid phase the fraction of mass in the struts is the parameter with a larger variation. When f_s was plotted against the foaming parameters (Figure 23), important changes were found. In order to see if these changes are related with a change in relative density, these two magnitudes have been represented in Figure 25.

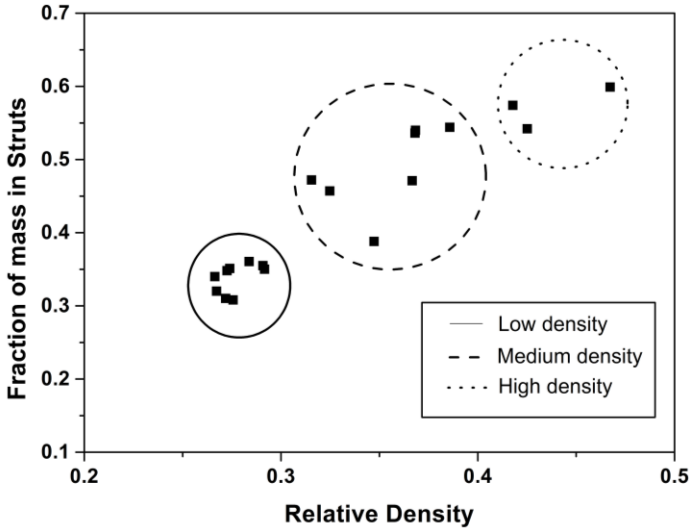

Figure 25. Fraction of mass in the struts as a function of relative density.

As it can be seen in the figure, f_s has a clear tendency with the relative density. Fraction of mass in struts is reduced as the relative density decreases. It means that struts become thinner when the density of the material is reduced.

These two effects, the constant thickness of the cell walls and the reduction of the thickness of struts with the decrease of the relative density, are not expected at all. Talking about cellular materials, it is common to found that when relative density is reduced, it results in a reduction of the cell wall thickness. For example, in PU foams, it has been observed that a reduction in ρ_r implies drainage from the cell walls to the struts [37]. The thinning continues until a minimum value at which coalescence starts to occur due to the breaking of cell walls.

The study of the solid part of these cellular materials highlights that a reduction of relative density in nanocellular foams results in totally different effects. A decrease in relative density results in a reduction of the struts thickness while cell wall thickness remains constant. This allows classifying the cellular materials of this paper into three groups, as it has been marked in Figure 25, high density foams, medium density foams and low density foams. These groups present clear differences in its cellular structure as it is shown in Figure 26.

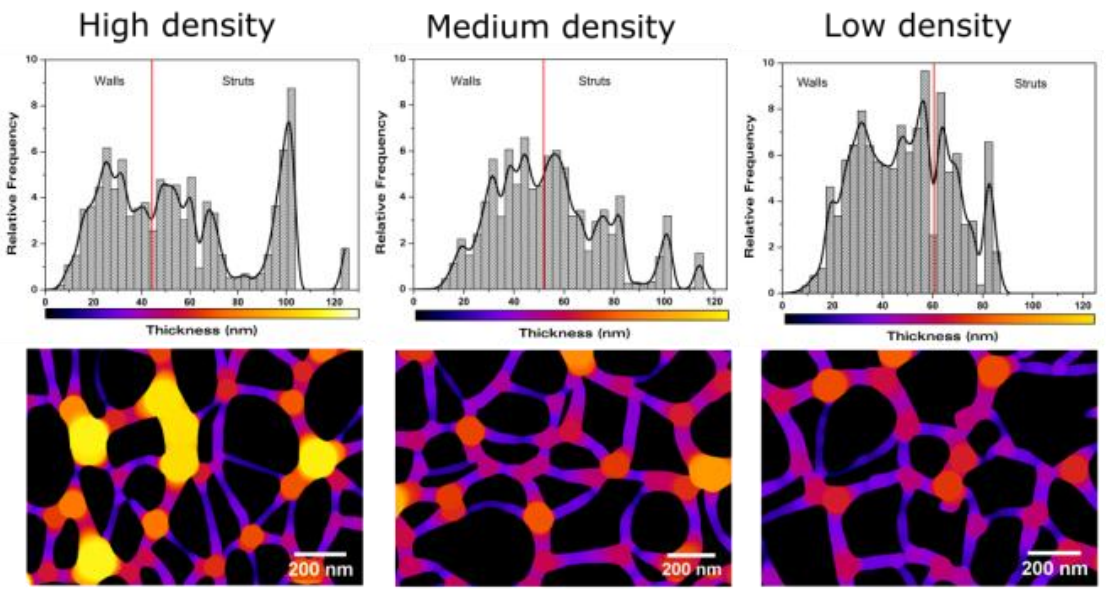

Figure 26. Solid phase distribution for high (Sample 1), medium (Sample 8) and low density samples (Sample 21).

The images show a material of each group. Samples presenting a high density present thick struts, and in the histogram it can be seen the wider distribution belonging to struts thickness. Struts distribution becomes thinner as relative density is reduced up to reach values of thickness very similar to that of the cell walls as it can be appreciated in the low density sample.

In summary, after the complete analysis of the cellular structure it has been proved that the key point in the density reduction of the nanocellular foams under study is the optimization of the foaming temperature. The increase of this temperature produces an increase in the number of nucleation points resulting in a reduction of density at almost constant cell size. In addition, this reduction produces other effects in the cellular structure of the cellular material such as the reduction of the struts thickness and the increase in the interconnectivity of the cellular structure.

5.2 Confinement Effect

The glass transition temperature has been measured for all the samples. As it can be seen when glass transition temperature of the first step of the nanocellular polymers are compared with the glass transition temperature of the solid precursor, there are differences up to 11ºC; while if the glass transition temperature of the second step of the nanocellular PMMA samples is compared with that of the solid precursor one, no significant differences are observed.

So it can be concluded that glass transition temperature of the nanocellular materials was higher than that of the bulk material (Table 1). This result has been previously reported and it has been attributed to a confinement effect of the polymer matrix [38,1] . The confinement effect is an important consequence of the evolution of the cellular materials from microcellular to nanocellular range. As it was seen in the introduction, the evolution from microcellular foams to

nanocellular foams implies an increase in the cell nucleation density, and a decrease of the cell size. All these effects results in a reduction in the thickness of the solid part of the cellular material (cell walls and struts).

When this thickness becomes of the same order of magnitude than the polymeric chain length, it appears what it is known as confinement effect. The polymeric chain is confined within the cell walls. This effect restricts the mobility of the polymeric chains resulting in an increase of its glass transition temperature.

Confinement effect has been recently demonstrated to be essential in the improvement of mechanical properties. Some works have demonstrated that nanocellular materials presents enhanced physical properties, modulus of elasticity, shore hardness… than that of the microcellular ones, and this seem to be due, in part, to the confinement effect.[5]

Figure 27.a. shows that although the cell wall thickness remains constant for all the samples, glass transition temperature increment (ΔT_g) increases as density is reduced. ΔT_g increases in a significant way, from 4ºC for high densities to 11ºC for low densities.

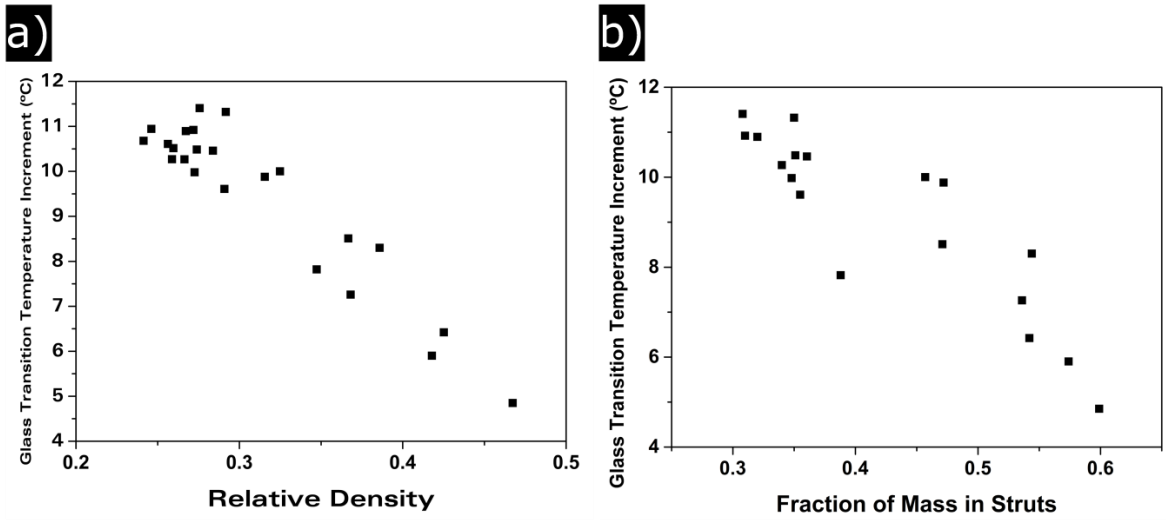

Figure 27. (**a**) Glass transition temperature increment as a function of relative density; (**b**) Glass transition temperature as a funtion of the fraction of mass in struts.

As it has been explained, confinement effect is produced as a result of a narrowing of the thickness of the different elements of the solid phase. So although cell wall thickness remains constant, struts reduce their thickness with the density reduction. As it is demonstrated in Figure 27.b. glass transition temperature increment depend on the fraction of mass in the struts. It means that glass transition temperature increases as struts become thinner.

So, in conclusion, confinement effect is present in all samples because thickness of the cell walls is of the same magnitude than PMMA molecular chains. However, higher density materials present thicker solids phase, located in the struts, this allows some mobility to the polymeric chains

located in these areas. As struts become smaller, the confinement starts to take place also in the struts. This implies an increase of the confinement effect with the thickness strut reduction, or what it is the same, with the relative density reduction.

In order to ratify this theory, thermal history of the samples was erased and then a second DSC cycle of heating was done. What it is observed is that the glass transition temperature measured in this step is almost the same than the bulk material one (Table 1). In fact, ΔT_{g_2} is close to 0 for all the material under study. This can be explained taking into account that the heating process used to erase the thermal history of the samples make disappear the nanocellular structure of the samples. This fact has been proved by heating Sample 8 in a furnace reproducing the DSC experiment. As it can be seen in Figure 28, sample does not present nanocellular structure after the heating cycle. The material has a relative density of 0.62, much higher than that of the original sample (0.33) and a microcellular structure in which the confinement effect does not take place.

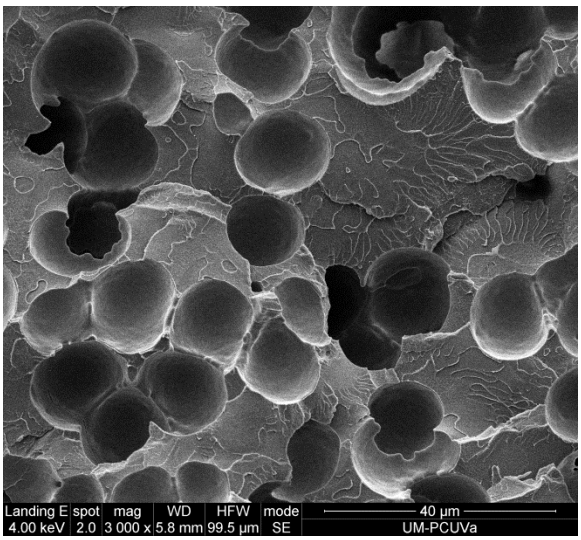

Figure 28. SEM micrograph of Sample 8 after the first DSC cycle.

6 Conclusions

Low density nanocellular PMMA has been produced by means of an optimization of the foaming parameters in the gas dissolution foaming process. A wide range of densities were obtained only by changing the foaming conditions, having nanocellular materials from 0.47 of ρ_r at 40ºC to really low relative densities of 0.24 at 90ºC of foaming temperature. These low density nanocellular materials have been achieved for the first time using a homopolymer as raw material, and using no extremely low saturation temperatures (saturation temperature was room temperature).

In addition, a complete analysis of the cellular structure, both gaseous phase and solid phase, has been carried out and this analysis has been correlated with the changes in relative density. In fact, a detailed analysis of process-density-structure, never done before for this type of materials, has been carried out. This correlation has led to important conclusions.

Relating to gaseous phase it has been found that the key factor in the reduction of relative density is the increase in the number of nucleation points, being possible to maintain the cell size constant as relative density is reduced. Moreover, it has been demonstrated that reducing relative density results in an increase of the interconnectivity of the cellular structure, achieving completely open structures for low relative densities. On the other hand, relating to the solid phase, it has been proved that unlike microcellular foams, cell wall thickness remains constant as relative density is reduced while struts size is reduced. Finally, it has been confirmed, that the production of nanocellular foams results in a confinement of the polymer chains within cell walls being this effect more important when the density is reduced. This fact can be proved by the increase of the glass transition temperature of nanocellular materials with respect to the bulk material one.

The results presented in this master Thesis has been recently submitted to the journal Polymers. The submitted paper is entitled: “Low density nanocellular polymers based on PMMA produced by gas dissolution foaming: fabrication and cellular structure characterization” and it’s currently under evaluation.

Bibliography

1. Notario, B., Pinto, J. & Rodriguez-Perez, M. a. Towards a new generation of polymeric foams: PMMA nanocellular foams with enhanced physical properties. *Polymer (Guildf).* **63,** 116–126 (2015).

2. Pinto, J., Dumon, M., Pedros, M., Reglero, J. & Rodriguez-Perez, M. A. Nanocellular CO2 foaming of PMMA assisted by block copolymer nanostructuration. *Chem. Eng. J.* **243,** 428–435 (2014).

3. Eaves, D. *Handbook of Polymer Foams*. (Rapra Technology Limited, 2004).

4. Saiz-Arroyo, C., de Saja, J. A. & Rodríguez-Pérez, M. A. Production and Characterization of crosslinked low-density polyethylene foams using waste of foams with the same composition. *Polym. Eng. Sci.* **52,** 751–759 (2012).

5. Notario, B., Pinto, J. & Rodriguez-Perez, M. A. Nanoporous polymeric materials: A new class of materials with enhanced properties. *Prog. Mater. Sci.* **78-79,** 93–139 (2016).

6. Miller, D. & Kumar, V. Microcellular and nanocellular solid-state polyetherimide (PEI) foams using sub-critical carbon dioxide II. Tensile and impact properties. *Polymer (Guildf).* **52,** 2910–2919 (2011).

7. Knudsen, M. *The Kinetic Theory of Gases*. (1934).

8. Gibson, L. J. & Ashby, M. F. *Cellular solids: Structure and Properties*. (Cambridge: Cambridge University Press., 1997).

9. Mills, N. J. Handbook of polymeric foams and foam technology. *Polymer (Guildf).* **34,** 2237 (1993).

10. Kumar, V. & Suh, N. P. A process for making microcellular thermoplastic parts. *Polym. Eng. Sci.* **30,** 1323–1329 (1990).

11. Sun, H. *et al.* Microcellular foams from some high-performance composites. *Polymer (Guildf).* **46,** 6623–6632 (2005).

12. Arora, K. A., Lesser, A. J. & McCarthy, T. J. Preparation and Characterization of Microcellular Polystyrene Foams Processed in Supercritical Carbon Dioxide. *Macromolecules* **31,** 4614–4620 (1998).

13. Kumar, V. & Weller, J. E. A Process to Produce Microcellular PVC. *Int. Polym. Process.* **1,** 73–80 (1993).

14. Parks, K. L. & Beckman, E. J. Genetration of Microcellular Polyurethane Foams via Polymerization in Carbon Dioxide . II : Foam Formation and Characterization. *Polym. Eng. Sci.* **36,** 2417–2431 (1996).

15. Xing, Z., Wu, G., Huang, S., Chen, S. & Zeng, H. Preparation of microcellular cross-linked polyethylene foams by a radiation and supercritical carbon dioxide approach. *J. Supercrit.*

Fluids **47,** 281–289 (2008).

16. Reglero Ruiz, J. A., Viot, P. & Dumon, M. Microcellular foaming of polymethylmethacrylate in a batch supercritical CO 2 process: Effect of microstructure on compression behavior. *J. Appl. Polym. Sci.* **118,** 320–331 (2010).

17. Weller, J. E. & Kumar, V. Solid_State microcellular Polycarbonate Foams.I The steady State Process Space Using Subcritical Carbon Dioxide. *Engineering* **47,** 21–25 (2007).

18. Shimbo, M., Higashitani, I. & Miyano, Y. Mechanism of strength improvement of foamed plastics having fine cell. *J. Cell. Plast.* **43,** 157–167 (2007).

19. Nadella, K. & Kumar, V. Tensile and flexural properties of solid-state microcellular ABS panels. *Exp. Anal. Nano Eng. …* 765–766 (2007). at <http://link.springer.com/chapter/10.1007/978-1-4020-6239-1_380>

20. Juntunen, R. P., Kumar, V., Weller, J. E. & Bezubic, W. P. Impact strength of high density microcellular poly(vinyl chloride) foams. *J. Vinyl Addit. Technol.* **6,** 93–99 (2000).

21. Collias, D. I., Baird, D. G. & Borggreve, R. J. . Impact toughening of polycarbonate by microcellular foaming. *Polymer (Guildf).* **35,** 3978–3983 (1994).

22. Costeux, S. CO_2 -blown nanocellular foams. *J. Appl. Polym. Sci.* **131,** n/a–n/a (2014).

23. Schmidt, D., Raman, V. I., Egger, C., du Fresne, C. & Schädler, V. Templated cross-linking reactions for designing nanoporous materials. *Mater. Sci. Eng. C* **27,** 1487–1490 (2007).

24. Notario, B. *et al.* Experimental validation of the Knudsen effect in nanocellular polymeric foams. *Polym. (United Kingdom)* **56,** 57–67 (2015).

25. Hentze, H. Template synthesis of porous organic polymers. *Curr. Opin. Solid State Mater. Sci.* **5,** 343–353 (2001).

26. Lazzari, M. & López-Quintela, M. A. Block Copolymers as a Tool for Nanomaterial Fabrication. *Adv. Mater.* **15,** 1583–1594 (2003).

27. Cheng, L.-P., Dwan, A.-H. & Gryte, C. C. Membrane formation by isothermal precipitation in polyamide-formic acid-water systems I. Description of membrane morphology. *J. Polym. Sci. Part B Polym. Phys.* **33,** 211–222 (1995).

28. Kiefer, J., Hilborn, J. G. & Hedrick, J. L. Chemically induced phase separation: a new technique for the synthesis of macroporous epoxy networks. *Polymer (Guildf).* **37,** 5715–5725 (1996).

29. Park, S. H. & Xia, Y. Macroporous Membranes with Highly Ordered and Three-Dimensionally Interconnected Spherical Pores. *Adv. Mater.* **10,** 1045–1048 (1998).

30. Cheong, S., Rachkov, A. E., Park, J.-K., Yano, K. & Karube, I. Synthesis and Binding Properties of a Noncovalent. *J. Polym. Sci.* **36,** 1725–1732 (1997).

31. Colton, J. S. the Nucleation of Microcellular Foams in Semi Crystalline Thermoplastics∗. *Mater. Manuf. Process.* **4,** 253–262 (1989).

32. Colton, J. S. & Suh, N. N. P. The nucleation of microcellular thermoplastic foam with additives: Part II: Experimental Results and discussion. *Polym. Eng. Sci.* **27,** 493–499 (1987).

33. Crank, J. *The mathematics of diffusion*. (Oxford University Press, 1975). doi:10.1016/0306-4549(77)90072-X

34. Wilfried, W. Model calculation of the temperature dependence of small molecule diffusion in high polymers. **63,** 1080–1085 (1968).

35. Guo, H. & Kumar, V. Solid-state poly(methyl methacrylate) (PMMA) nanofoams. Part I: Low-temperature CO2 sorption, diffusion, and the depression in PMMA glass transition. *Polymer (Guildf).* **57,** 157–163 (2015).

36. Pinto, J., Solorzano, E., Rodriguez-Perez, M. a. & de Saja, J. a. Characterization of the cellular structure based on user-interactive image analysis procedures. *J. Cell. Plast.* **49,** 555–575 (2013).

37. Pardo-Alonso, S. *et al.* 3D Analysis of the progressive modification of the cellular architecture in polyurethane nanocomposite foams via X-ray microtomography. *Eur. Polym. J.* **49,** 999–1006 (2013).

38. Reglero Ruiz, J. A., Dumon, M., Pinto, J. & Rodriguez-Pérez, M. A. Low-density nanocellular foams produced by high-pressure carbon dioxide. *Macromol. Mater. Eng.* **296,** 752–759 (2011).